Title

Numerical investigation of a joint approach to thermal energy storage and compressed air energy storage in aquifers

Authors

Guo, Chaobin
Zhang, Keni
Pan, Lehua
et al.

Publication Date

2017-10-01

DOI

10.1016/j.apenergy.2017.06.030

Peer reviewed

Numerical investigation of a joint approach to thermal energy storage and compressed air energy storage in aquifers

Author links open overlay panel ChaobinGuo[ad] KeniZhang[ab] LehuaPan[b] ZuansiCai[c] CaiLi[d] YiLi[e]
Show more

https://doi.org/10.1016/j.apenergy.2017.06.030

Highlights

- One wellbore-reservoir numerical model was built to study the impact of ATES on CAESA.
- With high injection temperature, the joint of ATES can improve CAESA performance.
- The considerable utilization of geothermal occurs only at the beginning of operations.
- Combination of CAESA and ATES can be achieved in common aquifers.

Abstract

Different from conventional compressed air energy storage (CAES) systems, the advanced adiabatic compressed air energy storage (AA-CAES) system can store the compression heat which can be used to reheat air during the electricity generation stage. Thus, AA-CAES system can achieve a higher energy storage efficiency. Similar to the AA-CAES system, a compressed air energy storage in aquifers (CAESA) system, which is integrated with an aquifer thermal energy storage (ATES) could possibly achieve the same objective. In order to investigate the impact of ATES on the performance of CAESA, different injection air temperature schemes are designed and analyzed by using numerical simulations. Key parameters relative to energy recovery efficiencies of the different injection schemes, such as pressure distribution and temperature variation within the aquifers as well as energy flow rate in the injection well, are also investigated in this study. The simulations show that, although different injection

schemes have a similar overall energy recovery efficiency (~97%) as well as a thermal energy recovery efficiency (~79.2%), the higher injection air temperature has a higher energy storage capability. Our results show the total energy storage for the injection air temperature at 80 °C is about 10% greater than the base model scheme at 40 °C. Sensitivity analysis reveal that permeability of the reservoir boundary could have significant impact on the system performance. However, other hydrodynamic and thermodynamic properties, such as the storage reservoir permeability, thermal conductivity, rock grain specific heat and rock grain density, have little impact on storage capability and the energy flow rate. Overall, our study suggests that the combination of ATES and CAESA can help keep the high efficiency of energy storage so as to make CAESA system more efficiency.

Keywords

Compressed air energy storage
Aquifer
Thermal energy storage
Injection air temperature

Nomenclature

η
: energy recovery efficiency

$\eta_{thermal}$
: thermal storage efficiency

C_p
: constant-pressure specific heat capacity (J/(kg·K))

E_{in}
: energy injected through wellhead

E_{out}
: energy produced through wellhead

H
: enthalpy (J/kg)

HE

heat exchanger

HPC
: high-pressure compressor

HPT
: high-pressure turbine

k_1
: gas storage reservoir permeability

k_2
: gas storage reservoir boundary permeability

LPC
: low-pressure compressor

LPT
: low-pressure turbine

m
: air mass (kg)

MPC
: media pressure compressor

P_0
: minimal capillary pressure (Pa)

P_{max}
: maximal capillary pressure (Pa)

S_g
: gas saturation

S_{lr}
: residual liquid saturation

S_{ls}
: saturated liquid saturation

S_{gr}
: residual gas saturation

T
: temperature (°C)

1. Introduction

The studies of compressed air energy storage (CAES) began in the late 1970s [1]. The first commercial CAES plant, the Huntorf plant (290 MW) in German has been successfully operated for almost 40 years since 1978 [2]. Another CAES plant in McIntosh Alabama (110 MW) [3] was built in 1991. However, as the nuclear power industry lost momentum, oil prices retreated from their peaks and with the development of gas turbines, the market conditions for CAES declined for a period [4]. Now with the growing concern about greenhouse gas emissions from fossil fuel utilization, interest has begun to grow in large-scale energy storage of renewable energy sources such as wind and solar.

Energy storage scale and efficiency are the two most important aspects that need to be considered in relation to CAES. For the energy scale aspect, different kinds of storage vessels have been investigated. Both of the existing commercial CAES plants use solution-mined salt caverns as the storage vessels [5], [6]. However, the locations where the renewable energy plants are located may not have the necessary geological conditions for feasible cavern development. Man-made caverns would significantly increase the cost of CAES, leading to diseconomy. This geological constraint limits the widespread development of this variant of CAES technologies [7]. Aquifers have been proved suitable for compressed air energy storage by field tests [8], analytical solutions [9] and numerical simulations [10], [11], [12], [13], [14]. Compressed air energy in aquifers (CAESA) has been widely accepted as alternative to achieve large-scale energy storage. Several projects have been proposed or are under construction, such as the Yakima Minerals Hybrid Plant in USA, Datang Inner Mongolia CAESA plant in China [4], [15].

The other aspect is the energy storage efficiency. The energy lost can occur in the charging stage, storage stage and discharging stage. Studies of compressor and turbine efficiency during charging and discharging stages have already been widely conducted for many years by different researchers [16], [17], [18]. The compression heat that produced during the compression process is wasted in the Huntorf CAES plant and this affects the total efficiency to a certain extent [19], [20]. The U.S. Department of

Energy conducted a series of feasibility studies and small-scale demonstration projects, with the aim to clarify the site selection and the second generation of CAES systems [8], [20]. Some thermal energy storage (TES) methods have been applied to CAES to recover the compression heat. With a heat recuperator, the efficiency of the McIntosh CAES plant has been improved to 54%, which is higher than the Huntorf CAES plant (42%) [20]. The improvement of thermal energy storage efficiency is one popular research topic on CAES [21]. The so-called AA-CAES (Advanced Adiabatic Compressed Air Energy Storage) systems are introduced and studied extensively in the literature [18], [22], [23], [24].

However, many challenges still exist for the TES, especially in regard to the cost and technical aspects. The practical efficiency of TES is relatively low. Wang et al. [25] calculated the average round trip energy efficiency of CAES with TES pilot plant and found it to be about 22.6%, which is relatively low for commercial application. In addition, their results [25] indicate that one of the effective methods for improving the efficiency is to recover more heat from TES. With the high efficiency of TES, the required pressurized storage container and material would involve significantly increased costs. For cavern-based CAES, the maximum inlet air temperature is limited due to the instability of the salt cavern at temperatures above 325 K [18].

The idea of combination of CAESA and ATES (thermal energy storage in aquifers) comes from the fact that aquifers can be used to store thermal energy and the allowed temperature can be much higher than in a cavern due to the support of solid particles. A recent modelling study suggested that a high temperature rock-bed based TES system could provide a viable alternative for thermal energy storage of concentrating solar power plant [26]. Thus, an ATES system can be combined with a CAESA system is proposed in the study (Fig. 1). The proposed CAESA with ATES consists of air compression unit, compressed air and thermal storage system (in aquifer), and electricity generation unit. The air compression unit includes a multi-stage air compressors and heat exchangers. The heat exchange system here (the dotted rectangular box in Fig. 1) aims to cool down the compressed air temperature to the target aquifers' temperature, and to store the thermal energy used during the electricity generation process. The electricity generation unit is composed of turbines and heat exchangers. The heat exchanger system is to reheat the compressed air which is released from the CAESA system with ATES before entering the turbine power generators.

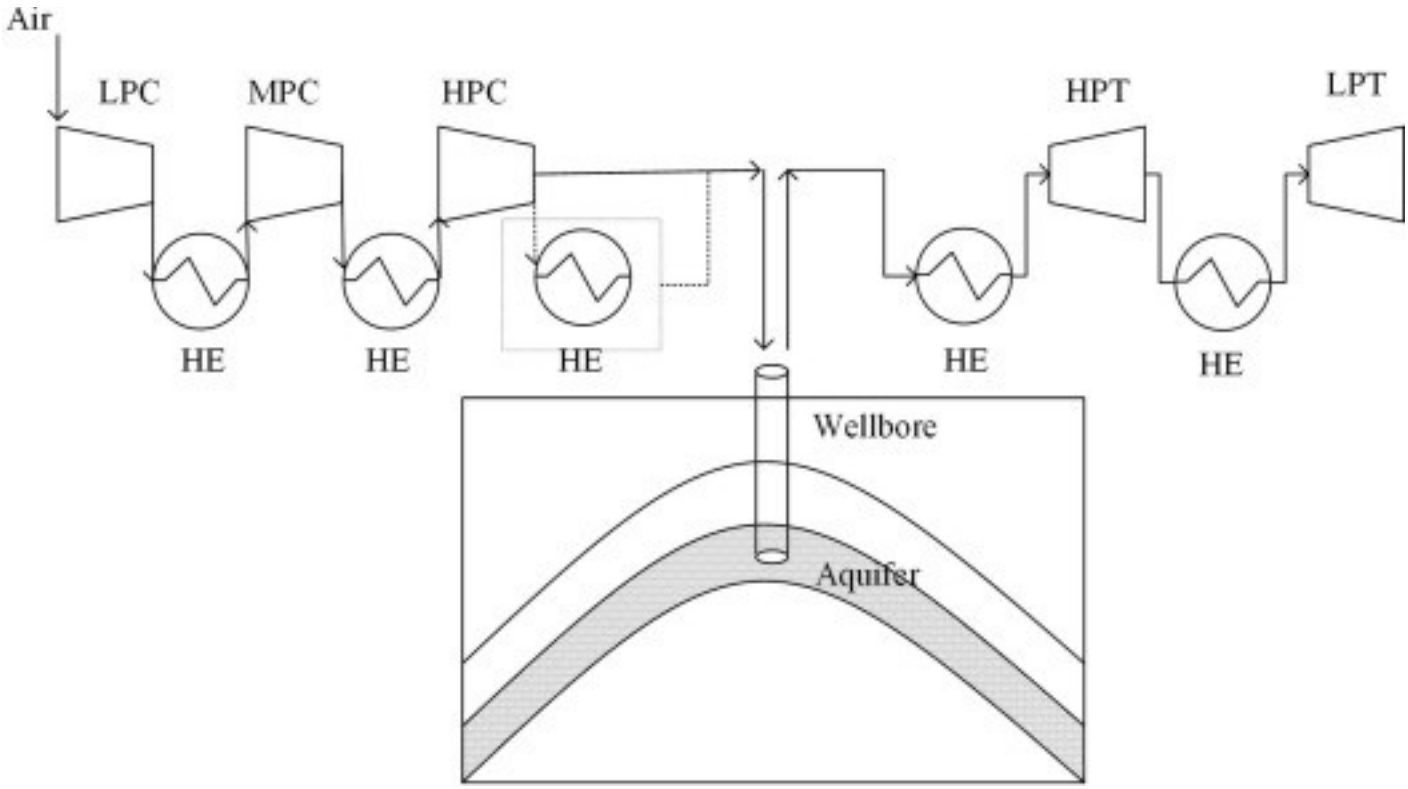

1. Download high-res image (113KB)
2. Download full-size image

Fig. 1. Schematic diagram of CAESA and ATES.

For the compressed air energy and thermal energy storage in aquifers, limit research has been reported to investigate the impact of the injection air temperature on overall energy recovery efficiency. In theory, higher temperature of the injection air means more thermal energy being stored in ATES. This will potentially improve overall energy recovery efficiency provided that the thermal energy storage in ATES system have a sufficiently high recovery rate. As an initial investigation of such novel energy storage system, a temperature range of 20–80 °C is selected for this study. This is because too high a temperature of the injection air may decrease the recovery efficiency due to high temperature gradient between surrounding groundwater. A recent study of a conventional ATES by injecting hot water showed that higher storage temperatures increase buoyancy flow and reduce recovery efficiency [27]. Another novelty of this combination study is the media that used for thermal energy storage in aquifers, which is compressed air while not the liquid water in the traditional ATES system.

The objectives of this study are twofold: (1) How does ATES affect the performance of CAESA? (2) What is the influence of injection air temperature on the energy recovery efficiency? To address these key scientific questions, numerical models were developed

to analyze the system performance in aspects of pressure, temperature and energy efficiency. In addition, sensitivity analysis is conducted to investigate the impacts of thermodynamic and hydrodynamic properties, such as the storage reservoir permeability, thermal conductivity, rock grain specific heat and rock grain density, on the system performance. These results can help to design the CAESA-ATES system.

2. Model setup

2.1. Conceptual model

Referring to the Huntorf CAES [28] plant for better comparison, we setup the CAESA system as shown in Fig. 3. The air storage reservoir, which is also called the air bubble area is characterized by a cylinder with the same air storage capacity and the same wellbore size as used in the Huntorf CAES plant. According to the typical properties of sandstones [4], [10], we choose 0.2 as the porosity of the air storage aquifer and 0.1 as residual water saturation. With the same volume of 140,000 m^3 and the same height of 150 m as the cavern for the Huntorf CAES plant, the radius of the air storage reservoir is 40.63 m. The permeability (k_1) of the air storage reservoir (gathering the main working gas) is 1.0×10^{-12} m^2 and the permeability (k_2) of the boundary area is 1.0×10^{-20} m^2, which is extremely low as a sealant layer. The diameter of the operation well is 0.53 m, the same size as it in the Huntorf CAES plant. This conceptual model may represent a simplified form of an anticline, lenticel or closed fault structure. The most suitable structures are the anticline structures with closed boundary in Fig. 1or the depleted oil and gas fields. Some other geological structures that can also be simplified to the conceptual model are shown in Fig. 2. For the ATES system, there is no other special modification of the CAESA system since the same operation wellbore and aquifers are used as the storage media.

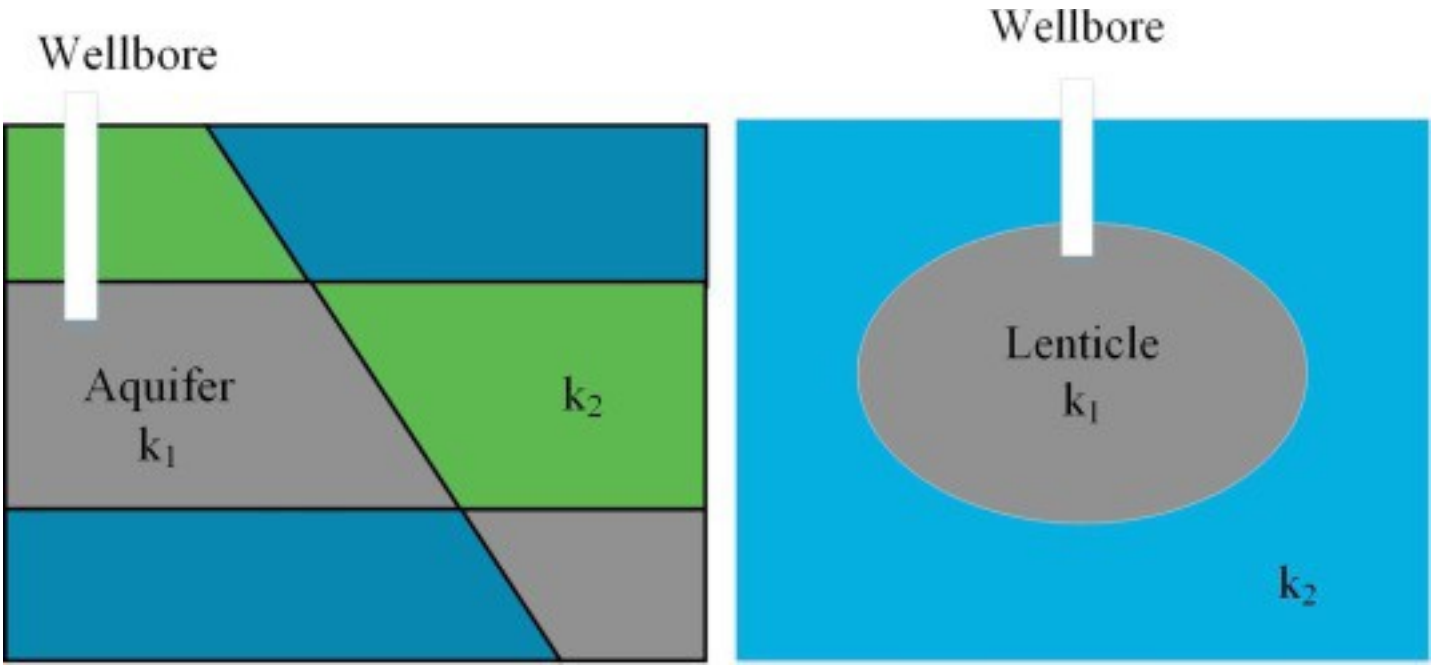

1. Download high-res image (60KB)
2. Download full-size image

Fig. 2. Schematic of suitable structures for compressed air energy storage (left to right refer to closed fault and lenticle).

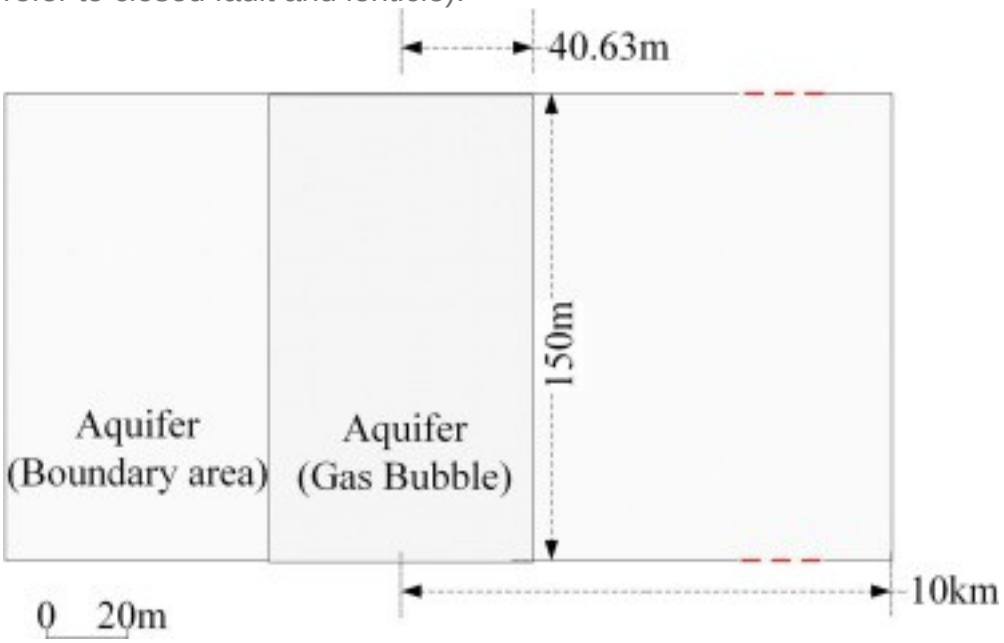

1. Download high-res image (97KB)
2. Download full-size image

Fig. 3. Conceptual model of CAESA.

2.2. Numerical model

2.2.1. T2Well/EOS3

The T2Well/EOS3 simulator, which is developed by Lehua Pan [29] based on TOUGH2, is used to carry out the investigation. The T2Well is a numerical simulator for solving the equations of non-isothermal, multiphase, and multi-component flow in an integrated wellbore-reservoir system, for a variety of applications. The EOS3 module describes the system consisting of H_2O-Air-Heat components in a porous or fractured media [30]. The simulator has been verified in the literatures [10], [11], [31] by comparisons of simulation and monitor results of the Huntorf CAES plant.

The domain is discretized using integral finite difference method with Wingridder [32]. It has total 4472 grids and 8797 connections. In vertical, the reservoir is discretized into layers in different thickness. The grids at the locations of wellhead, interface between overlying boundary and target aquifer have been refined. In horizontal, the reservoir is discretized into a radially symmetric mesh with lateral resolution varying from 0.1 m near the wellbore to 500 m in the far-field (see Fig. 4).

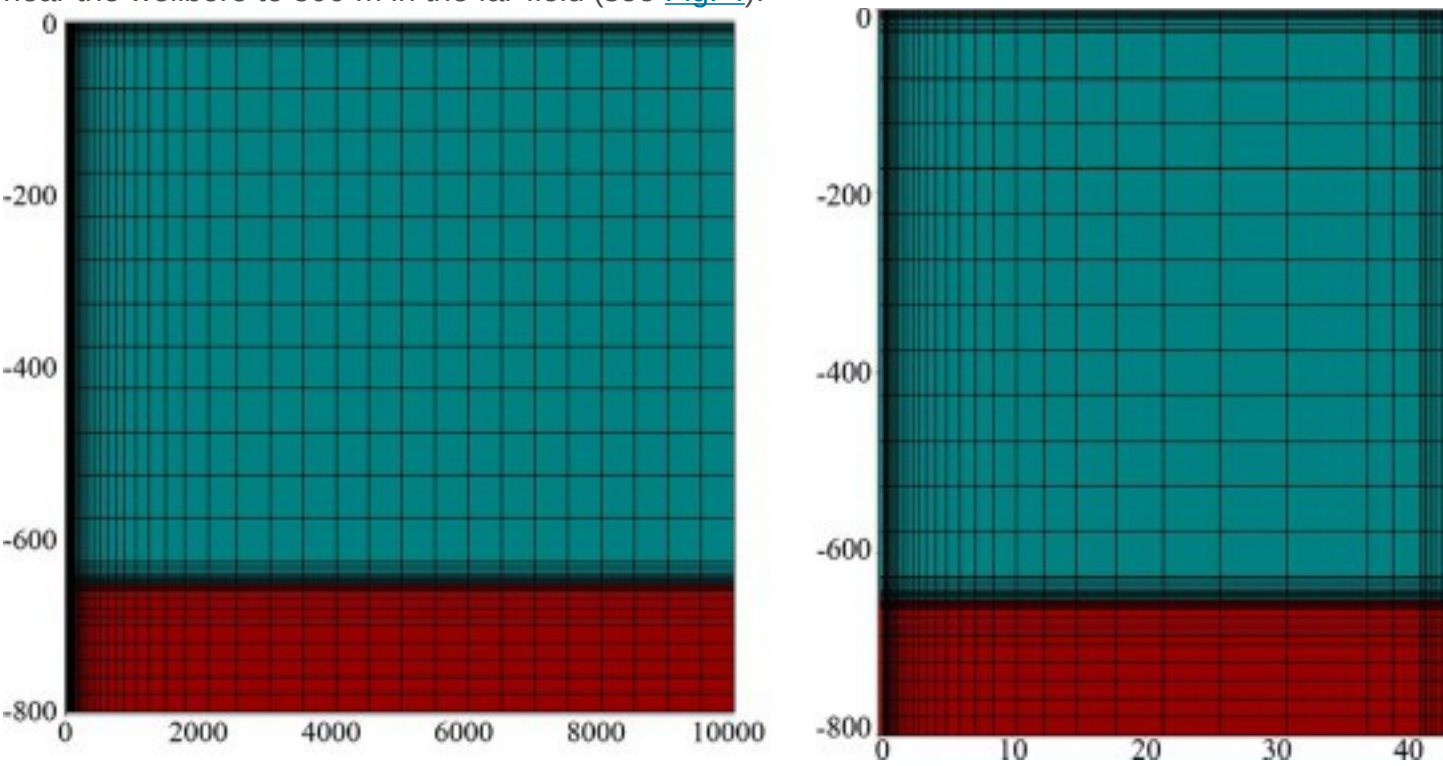

1. Download high-res image (218KB)
2. Download full-size image

Fig. 4. Domain discretization (left) with wellbore refinement (right).

The typical sandstone properties selected to represent the aquifers are shown in Table 1.

Table 1. Aquifers properties.

Parameters	Value	Unit
Grain density	2600	kg/m^3
Permeability ($k_x = k_y = 10\ k_z$)	1.0×10^{-12}	m^2
Porosity	0.2	–
Compressibility	1.0×10^{-10}	Pa^{-1}
Heat conductivity (fully liquid-saturated)	2.51	W/(m·°C)
Grain specific heat	920	J/(kg·°C)
Relative permeability function	van Genuchten-Mualem model	
λ	0.60	
S_{lr}	0.12	
S_{ls}	1.00	
S_{gr}	0.05	
Capillary pressure function	van Genuchten function	
λ	0.60	–
S_{lr}	0.10	–
P_0	675.68	Pa
P_{max}	5.0×10^5	Pa
S_{ls}	1.00	

2.2.2. Initial and boundary conditions

The initial pressure distribution is in hydrostatic equilibrium with atmospheric pressure at the top boundary (ground surface). The ground temperature is 15 °C and geothermal gradient is 31.25 °C/km (15 °C at the wellhead and 40 °C at the well-bottom). The gas bubble, which is assumed to be well developed, consisted of compressed air and residual water. Ideal gas bubble development can be achieved under the condition of anticline structure, lenticle structure and some faults. The other parts of the model (the boundary area) are saturated with water.

The upper, lower and outermost boundaries of the whole model are closed with no flow and heat conduction. The injection and production operations are achieved through the wellhead. The injection air temperature is fixed with a specified enthalpy.

3. Scheme design and simulation results

Part or all of the compression heat that produced by the last stage of the compressor contributes to the thermal energy that is going to be stored in aquifers. This part of the

thermal energy can be represented by different air temperature. A temperature range of 20–80 °C is selected for the studies. Different schemes are designed to analyze the impact on the energy storage scale and efficiency, as shown in Table 2. The temperature of 40 °C is selected as the base model temperature which is similar to the Huntorf CAES plant, and the higher temperature schemes are set as 60 °C and 80 °C. The temperature of 20 °C is selected as the low temperature scheme in which the colder air may be heated by the warmer formation resulting in harvesting of geothermal energy.

Table 2. Different injection air temperature schemes.

Parameters	Value				Unit
Temperature	20	40	60	80	°C

The working cycle is designed as daily cycle, as shown in Table 3. The injection and production rates are calculated based on the operation data of the Huntorf CAES plant [2], [10], [31].

Table 3. Daily cycle schedule.

Parameters	Value				Unit
Time	0.0–12.0	12.0–16.5	16.5–19.5	19.5–24.0	h
Injection/Production rate	54	0	−216	0	kg/s

3.1. Pressure and temperature distribution in the reservoir

Fig. 5 shows the pressure distribution near the air storage reservoir area after 300 cycles. Due to the low permeability of the boundary area, the maximal pressure builds up at the boundary of the air storage reservoir. For example, the pressure contour of 8.0 MPa appears at the boundary of the air storage reservoir (x = 40.63 m), as shown in Fig. 5(a). With the injection air temperature increasing from 20 °C to 60 °C, the upper boundary of 8.0 MPa pressure contour extends from about −720 m to −705 m, which indicates a slight increase in the average pressure in the air storage reservoir area.

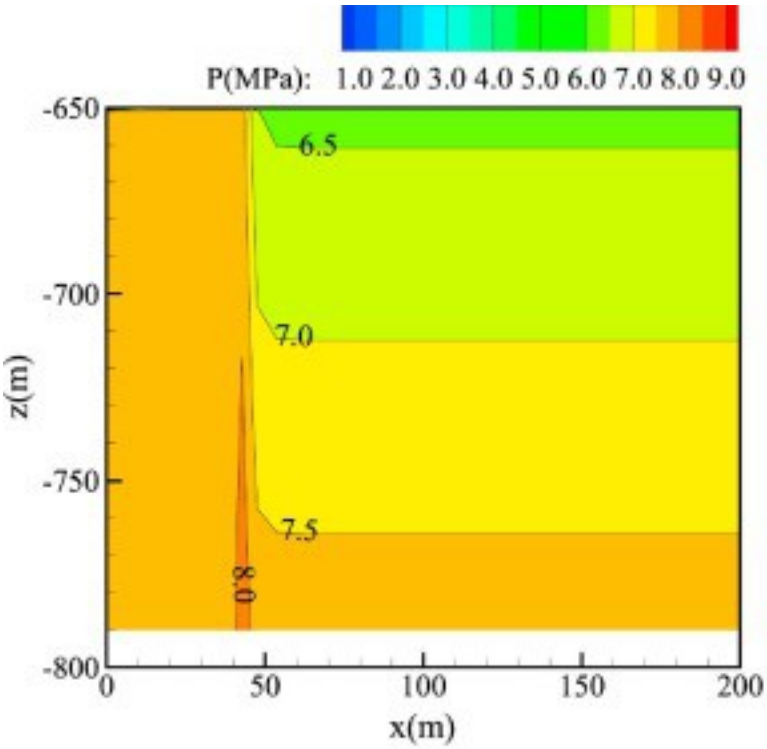

(a) 20 °C

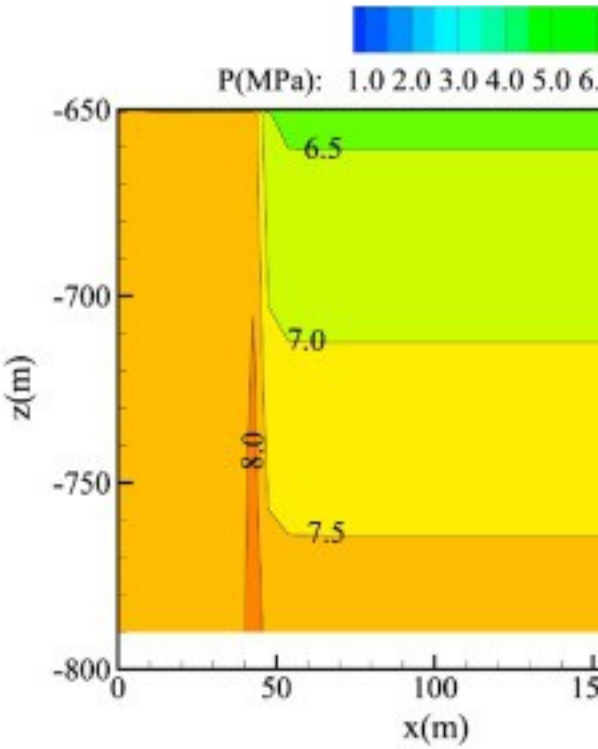

(b) 40 °C

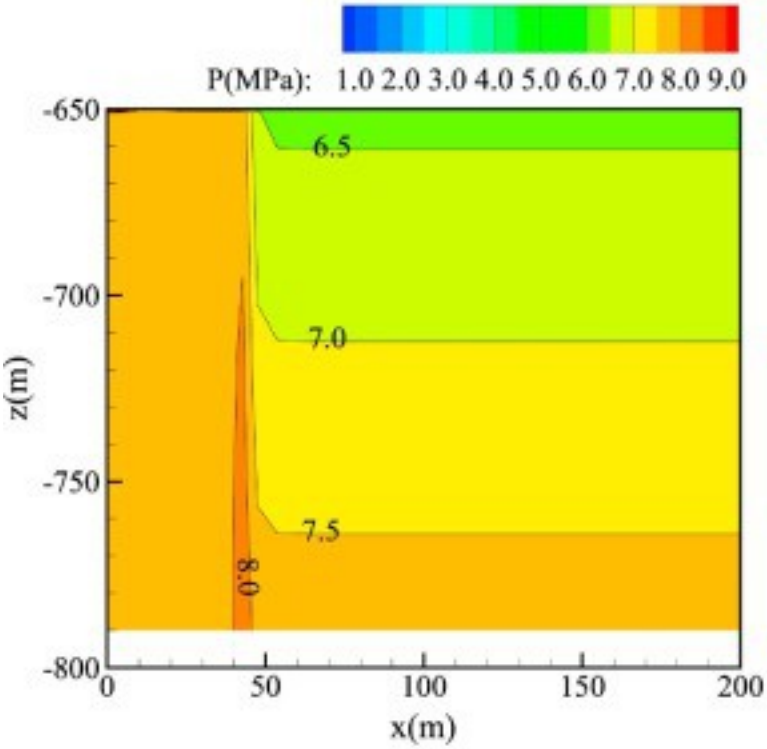

(c) 60 °C

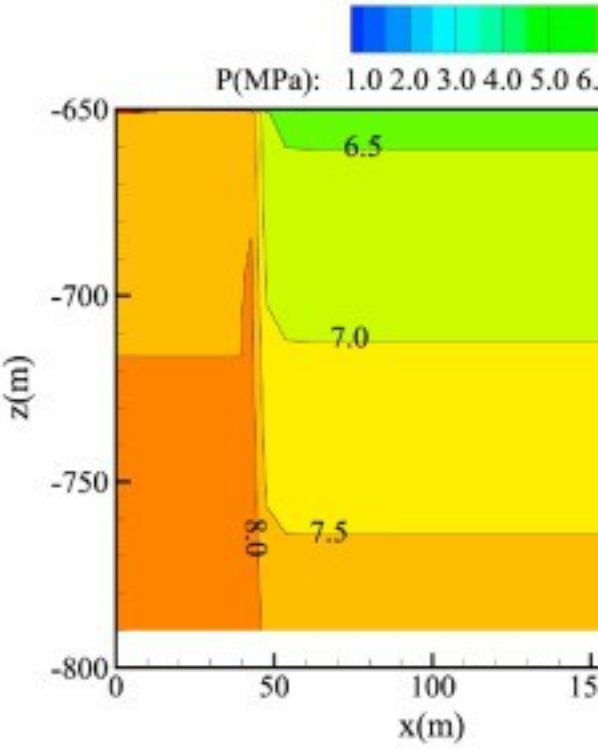

(d) 80 °C

1. Download high-res image (397KB)
2. Download full-size image

Fig. 5. Pressure distribution after 300 cycles.

The detailed pressure variation is shown in Fig. 6. For all schemes, the maximum and minimum pressure of one daily cycle gradually increase as the operation cycles continue. For instance, the maximal pressure after 300 cycles at 80 °C is about 8.92 MPa and the pressure is lower than 8.92 MPa at the beginning of the cycle. This is because the energy injected into the system is larger than produced. For one cycle, the pressure is higher during operation stages at a higher injection air temperature.

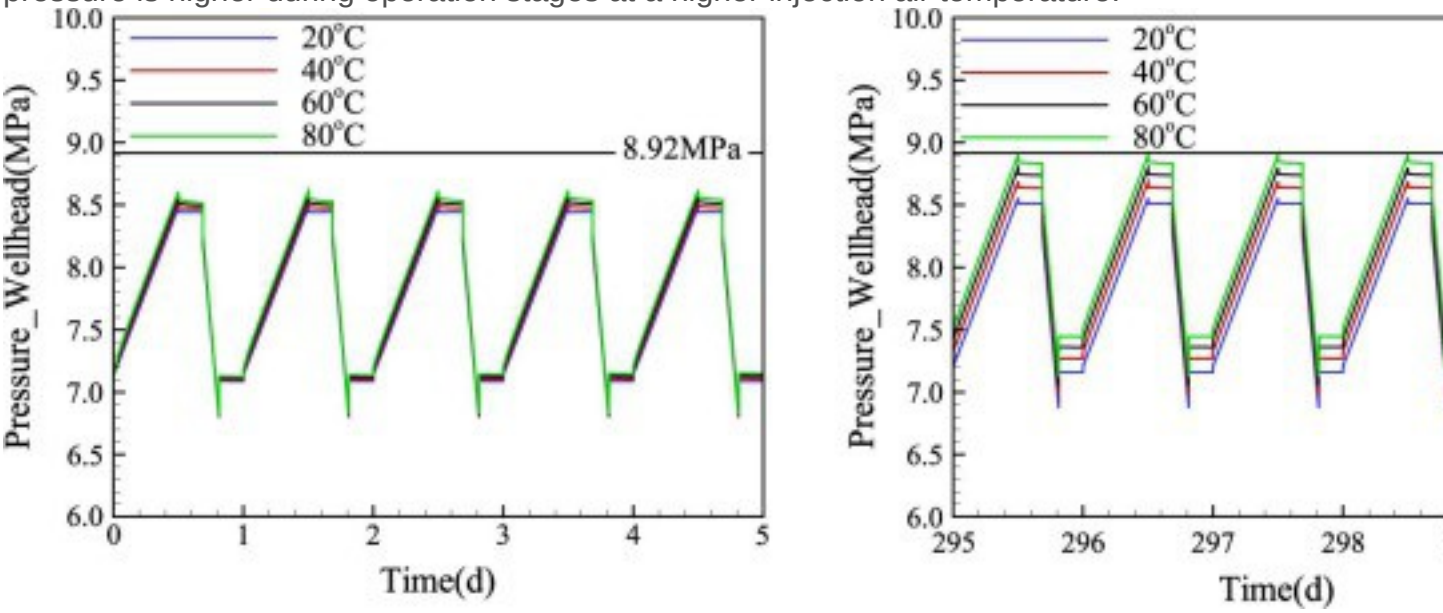

1. Download high-res image (139KB)
2. Download full-size image

Fig. 6. Pressure variation during 0–5 cycles (left) and 295–300 cycles (right).

The initial air temperature in the air storage reservoir is about 40 °C. After 300 cycles, for the low temperature (20 °C) scheme, the temperature distribution, shown in Fig. 7(a), indicates that the influence range (the 40 °C contour line) is about 20 m from the injection well. With the same injection air temperature (40 °C) as the initial air temperature, the temperature distribution exhibits little difference due to geothermal gradient. As for the high air temperature schemes, the influence radius is about 25 m for the 60 °C scheme and 28 m for the 80 °C scheme. The larger influence range, which means that more thermal energy is stored through the compressed air, is caused by the larger temperature difference under the same heat conductivity.

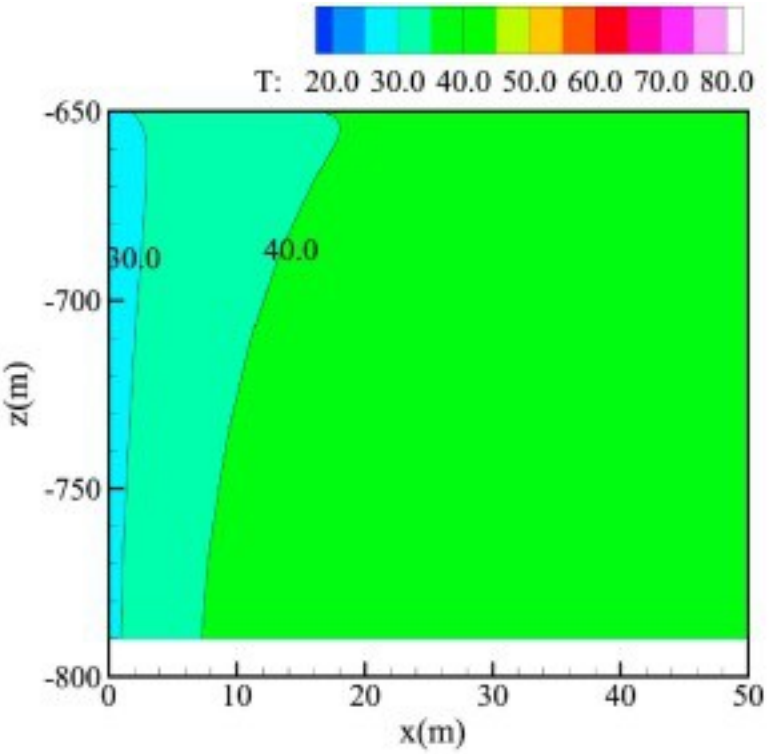

(a) 20 °C

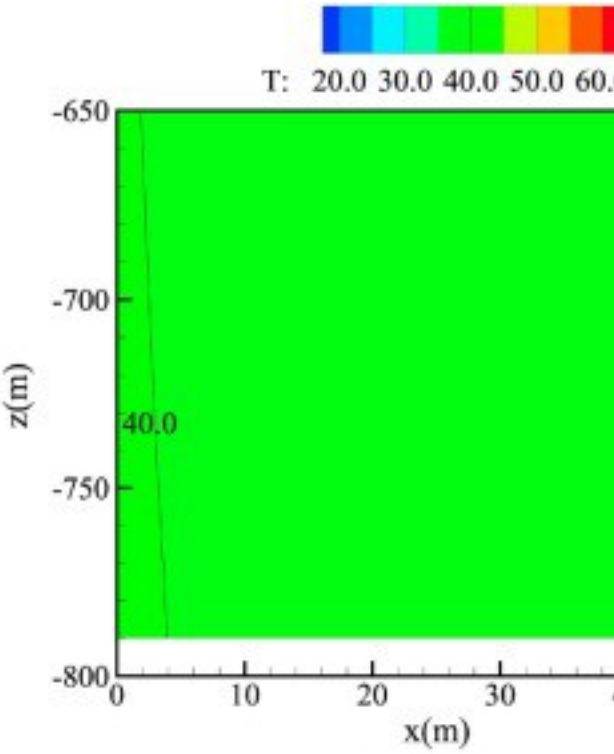

(b) 40 °C

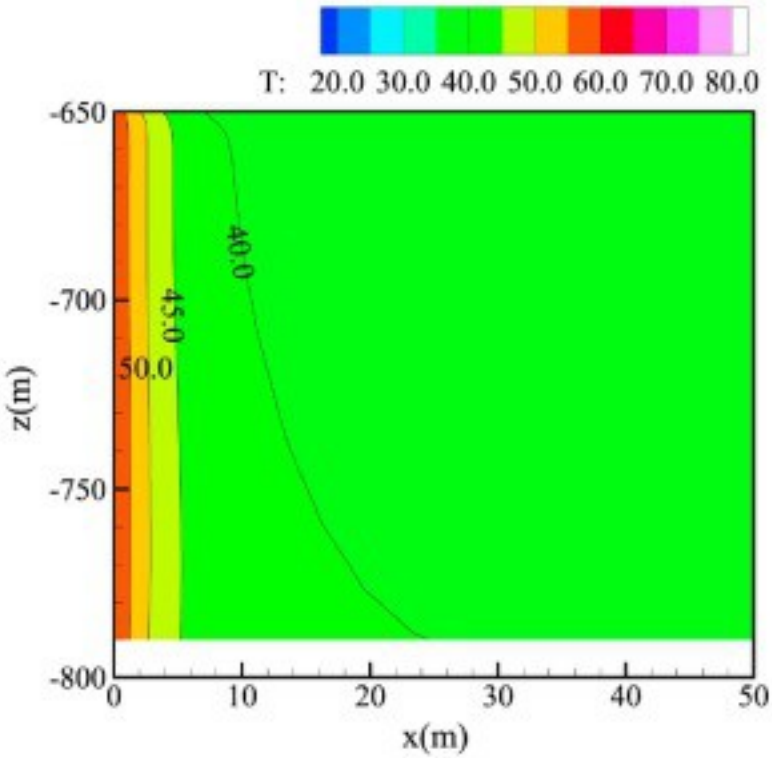

(c) 60 °C

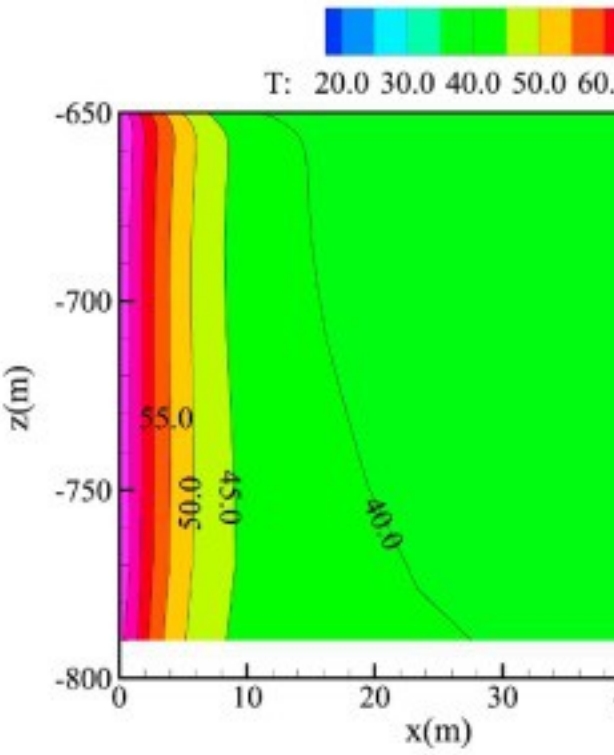

(d) 80°C

1. Download high-res image (387KB)
2. Download full-size image

Fig. 7. Temperature distribution after 300 cycles.

The wellhead temperature variation is shown in Fig. 8. The initial temperature of the wellhead is 15 °C and gradually increases to the injection air temperature during the first injection stage. During the shut-in stage, the temperature decreases slightly due to the heat lost to surrounding colder aquifers. During the production stage of the high-temperature schemes, the temperature decreases because of the expansion cooling effects. However, for the low temperature scheme (20 °C) the temperature increases during the production stage. This is because the impact of heat gain from the warmer reservoir is greater than the expansion cooling effects. In this situation, the production of compressed air withdraws not only the energy that is injected by the compressed air, but also the geothermal energy from aquifers. However, from Fig. 8(b) we can see that the maximal temperature for the 20 °C scheme decreases to a stable level as cycles continue. About a 5 °C temperature difference exists between the injection air and production air. This means that the effect of geothermal energy utilization is slight.

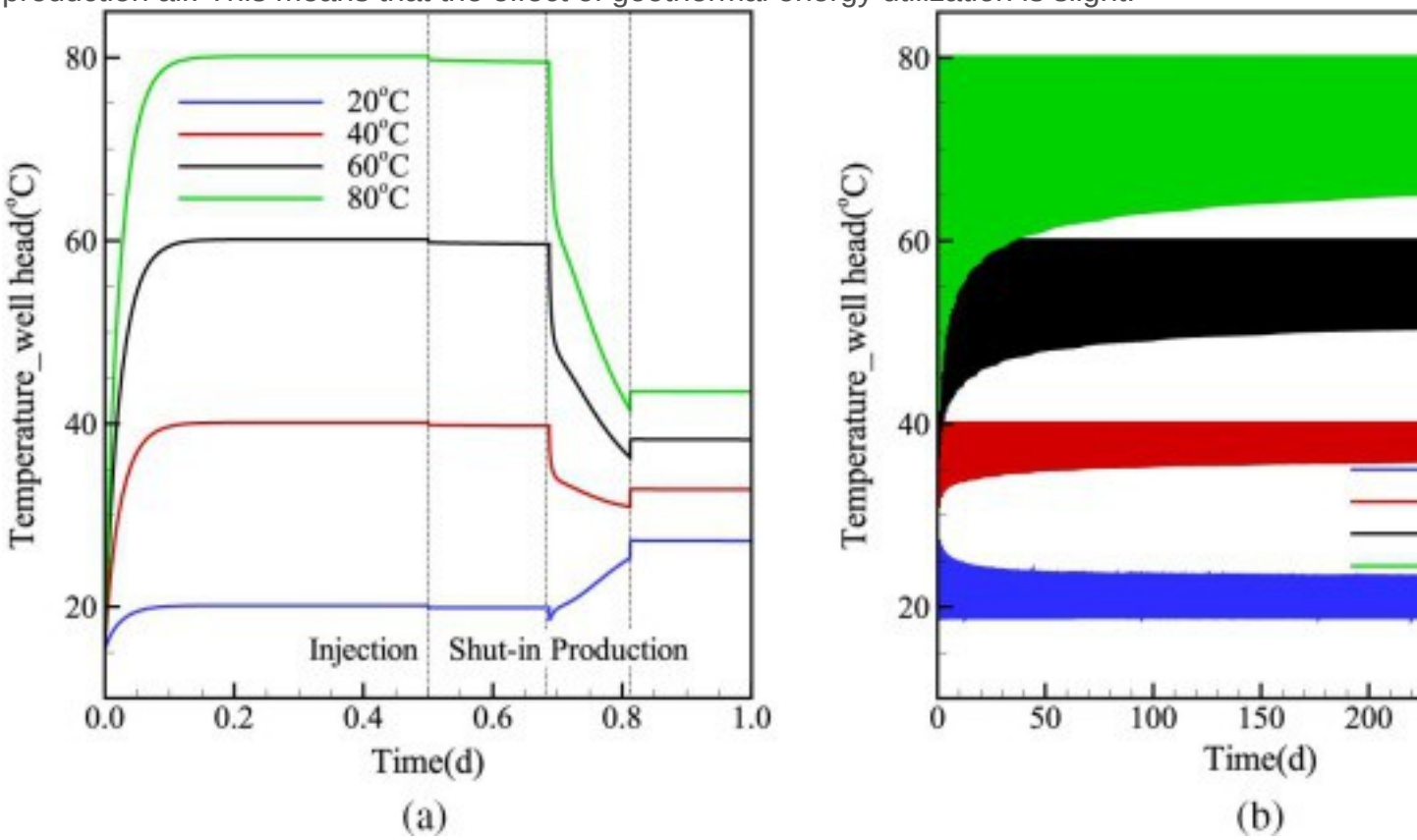

1. Download high-res image (132KB)
2. Download full-size image

Fig. 8. Temperature (wellhead) variation of the first cycle (a) and 300 cycles (b).

For high-temperature schemes, the maximal temperature at the wellhead is the injection temperature which remains the same during the 300 cycles, while the minimal temperature (the lowest production temperature) gradually increases to one relatively stable value as cycles continue. At the beginning of the cycles, a portion of heat is lost to aquifers through the wellbore due to the temperature difference between the wellbore and surrounding formations. As cycles continue, the heat loss rate decreases, represented by the relatively stable temperature. The results of the high-temperature schemes indicate that the considerable energy loss occurs at the beginning of operation cycles and the energy loss rate gradually decreases as cycles continue.

3.2. Energy flow rate and recovery efficiency

Energy recovery efficiency is defined as the ration of energy produced to energy injected through the wellhead during one cycle or the whole operation cycles:

$$\eta = E_{out}/E_{in}$$

Fig. 9 shows the energy flow rate at the wellhead during one cycle. A negative value indicates energy production. More energy is injected and produced through the wellhead with larger injection air temperature. For the basic model (40 °C), the total energy produced during 300 cycles is about 7.41×10^{11} J. More energy can be produced for the high injection air temperature. For example, the total energy produced for the 80 °C scheme is 8.21×10^{11} J, 10.80% higher than the 40 °C scheme.

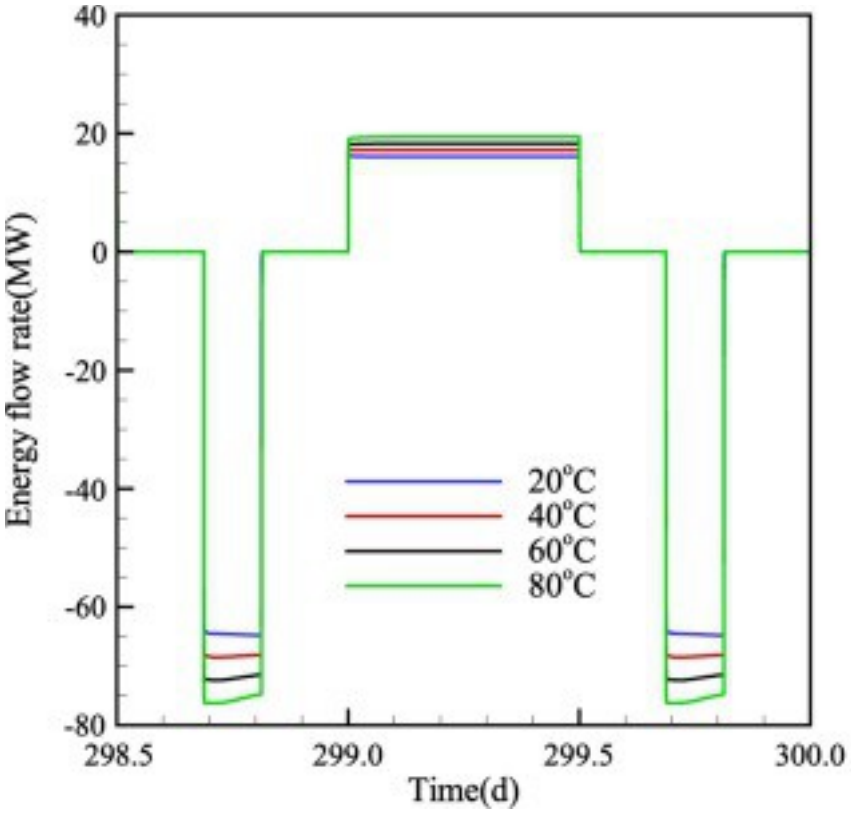

1. Download high-res image (90KB)
2. Download full-size image

Fig. 9. Wellhead energy flow rate variation.

Fig. 10 shows the energy recovery efficiency for different injection air temperature schemes. At the beginning of operations, the efficiency of the 20 °C scheme is higher than 100% due to the high initial temperature (40 °C) of air in the air storage reservoir. As cycles continue, the efficiency decreases to about 103%, which means that the considerable advantage of geothermal utilization can only be sustained for a short period, but it maintains slight efficiency improvement over the long term. This conclusion is consistent with the aforementioned temperature results.

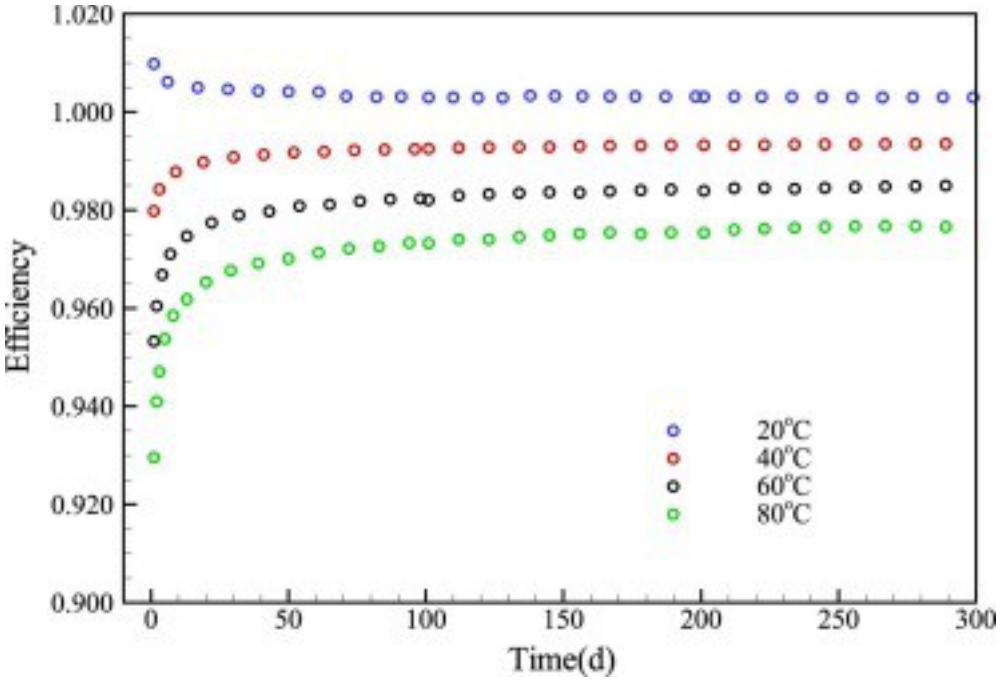

1. Download high-res image (107KB)
2. Download full-size image

Fig. 10. Energy recovery efficiency comparison of different injection air temperature.

For the high injection air temperature schemes (60 °C and 80 °C), the efficiency at the beginning of operation is a little lower than in later cycles. This is because the injection air temperature is higher than the initial temperature distribution in the wellbore and aquifers, and part of the injected thermal energy is transferred to the surrounding aquifers. The higher the injection air temperature, the more the energy transferred to aquifers and cannot be produced leading to the lower energy recovery efficiency. The heat transfer rate between the wellbore and surrounding aquifers decreases as the temperature difference reduced with the operation cycles. The energy recovery efficiency stabilized at 99%, 98% and 97% for the 40 °C, 60 °C and 80 °C schemes, respectively. The results indicate that aquifers have good thermal energy storage capacity even with the high temperature.

Even though the total energy recovery efficiency decrease as the injection air temperature increase, the efficiency difference is small. The total energy produced in the higher temperature (80 °C) scheme is 10.80% higher than in the 40 °C scheme. The stored total thermal energy can be calculated by the specific constant-pressure heat capacity and air mass, which is

$$\Delta H(thermal,in)=m\times Cp\times dT=54.00kg/s\times 12h\times 1.08\times 103J/(kg°C)\times(80°C-40°C)=1.01\times 1011J$$

Assuming that the compressed air energy (excluding the thermal energy) in 80 °C is produced with the efficiency of 40 °C (99%), the produced thermal energy is

$$\Delta H(thermal,out)=\Delta H(total,out)-\Delta H(air,in)\times 99\%=8.21\times 1011J-7.41\times 1011J=0.80\times 1011J$$

Thus, the recovery efficiency of thermal energy is

$$\eta thermal=\Delta H(thermal,out)/\Delta H(thermal,in)=79.20\%$$

From the calculation results, we may conclude that the higher injection air temperature performs better with regard to energy storage, considering the temperature range that the subsurface facilities can tolerate. In another words, if ATES is combined with a CAESA system, high efficiency will be expected for the CAESA system.

4. Discussion

4.1. Impact of hydrodynamic parameters on system performance

In the idealized basic model, the boundary of the gas storage reservoir is presumed to be impermeable, which may be impractical. This assumption will affect the performance of energy recovery. In order to investigate the impact of gas storage reservoir boundary permeability, several schemes are designed, as shown in Table 4.

Table 4. Schemes design of different gas storage reservoir boundary permeability (k_2).

Parameters	Value			Unit
k_1	1.00×10^{-12}			m^2
k_2	1.00×10^{-20}	1.00×10^{-15}	1.00×10^{-13}	m^2

After 300 cycles, the energy flow rate of higher k_2 is smaller, as shown in Fig. 11. This is because the deliverability of working fluid under high permeability is better than under low permeability and the gas and pressure migrate further away from the well. That part of the energy cannot be recovered during the production stage. In the meantime, water might be produced due to significant air migration further away from the well. Water production may cause damage to ground facilities. The smaller k_2 keeps more energy near the wellbore and offers the best energy recovery performance. However, a smaller k_2 may also produce an unfavoured effect, e.g. the difficulty to extend the energy storage scale.

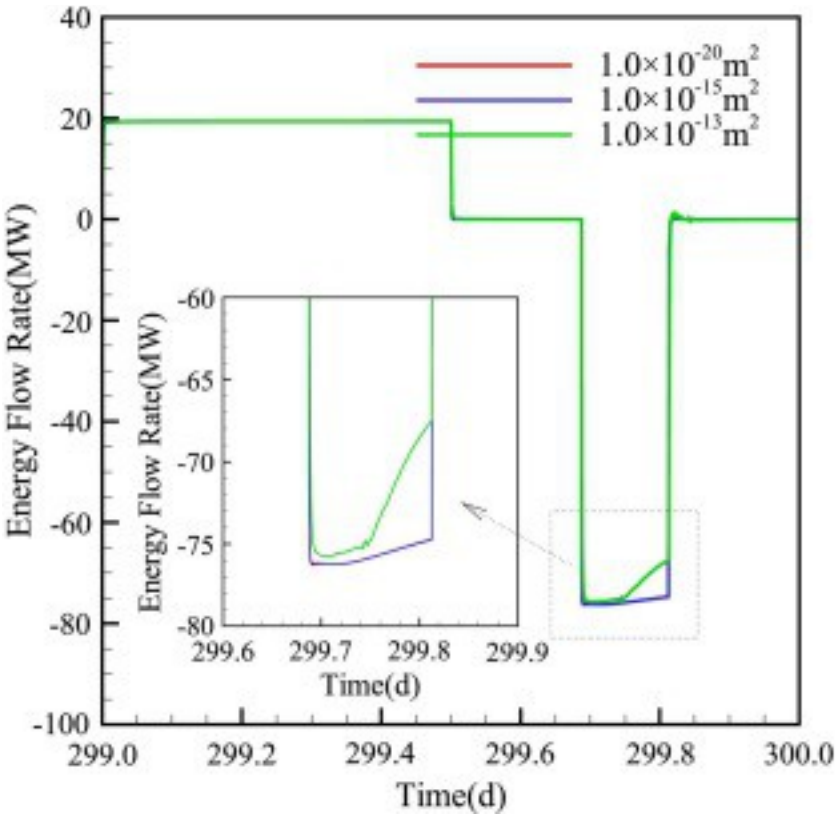

1. Download high-res image (142KB)
2. Download full-size image

Fig. 11. Energy flow rate for different air storage reservoir boundary permeability schemes.

For the investigation of the impact of gas storage reservoir permeability, schemes are designed as shown in Table 5.

Table 5. Scheme design of different gas storage reservoir permeability (k_1).

Parameters	Value				Unit
k_1	1.00×10^{-14}	1.00×10^{-13}	1.00×10^{-12}	5.00×10^{-12}	m^2
k_2	1.00×10^{-20}				m^2

The specific amount of compressed air (216 kg/s) cannot be produced under a low permeability (1.00×10^{-14} m^2) scheme, which indicates that the CAESA has a low limit of permeability. Under this permeability condition, the ATES also cannot be implemented. The low limit of permeability differs according to the storage scale. For the other k_1 schemes, the results of energy flow rate through the wellbore are shown in Fig. 12. After 300 cycles, the energy flow rate under different permeability schemes is almost the same except at the beginning of production. From the inserted figure in Fig. 12, we can observe that the higher the permeability, the slightly better the of energy recovery

performance. This is because the temperature of the higher permeability scheme decreases slower at the beginning of production than in the lower permeability scheme, as shown in Fig. 13. At the beginning of production, the fixed production rate can be achieved under the pressure difference, which is larger for a lower permeability scheme based on Darcy's Law. The sudden pressure drop under low permeability will cause the air to expand and the temperature to drop. When the air from aquifers flows through the wellhead, its temperature will increases within a short time.

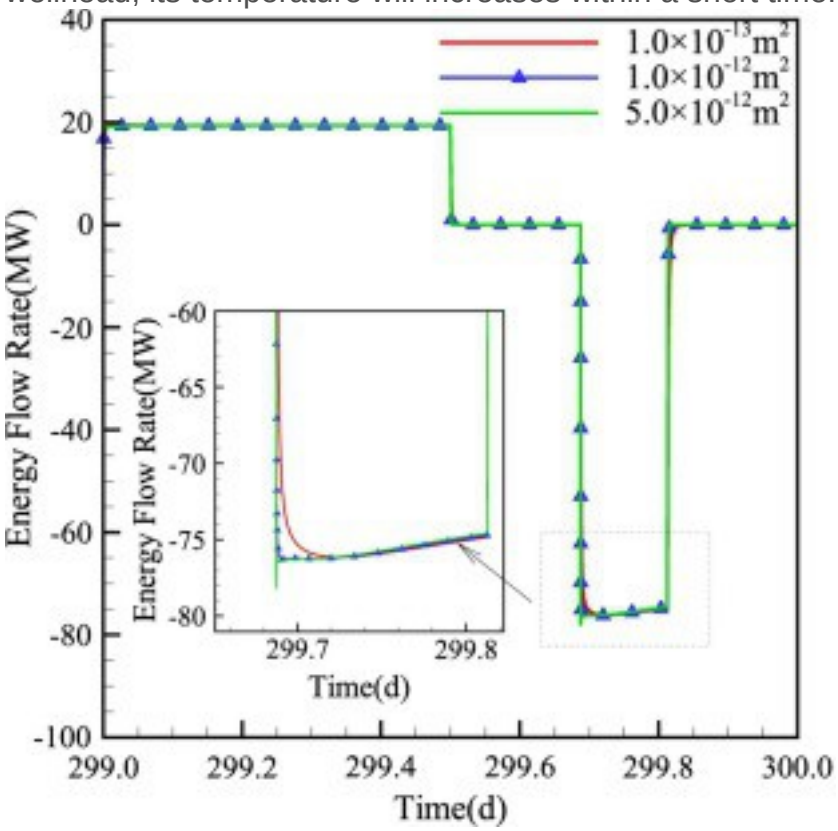

1. Download high-res image (137KB)
2. Download full-size image

Fig. 12. Energy flow rate of different air storage reservoir permeability schemes.

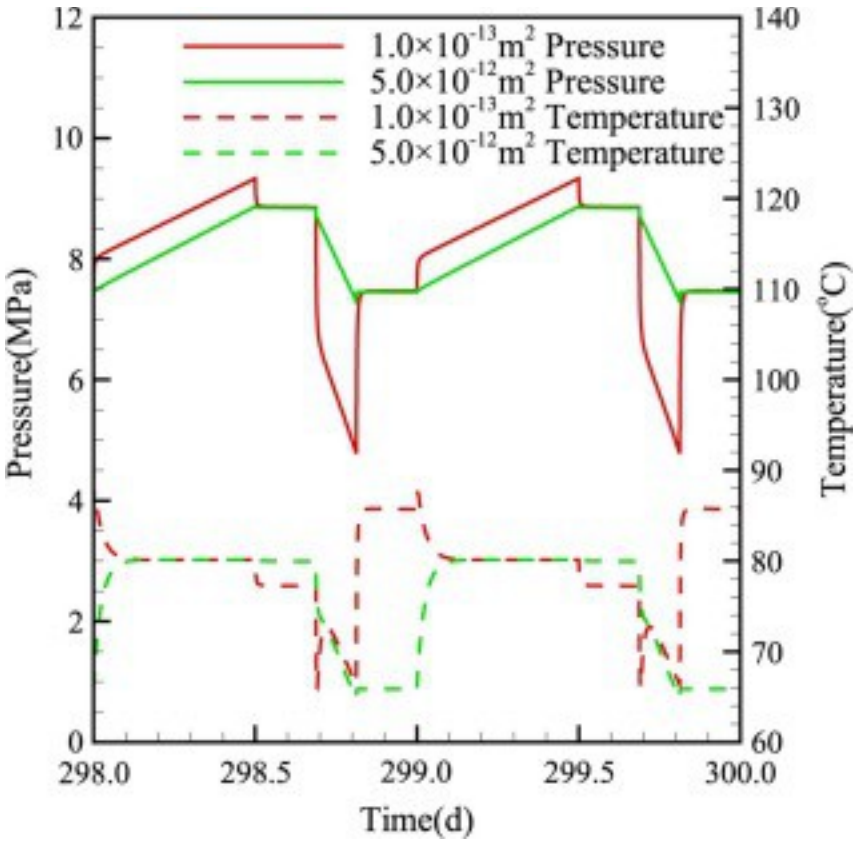

1. Download high-res image (153KB)
2. Download full-size image

Fig. 13. Pressure and temperature comparison of different air storage reservoir permeability schemes.

From the results of different air storage reservoir permeability schemes, we can see that the performance of energy production is similar for different schemes when a specific production rate can be achieved. However, the pressure and temperature variation under different air storage reservoir permeability schemes are quite significant.

4.2. Impact of thermodynamic parameters on system performance

The conduction of heat in aquifers is governed by their thermal properties: the volumetric heat capacity (indicative of the amount of temperature change that occurs when the aquifer media absorbs or loses a specific amount of energy) and the effective thermal conductivity (the ability of the aquifer media to transmit heat) [33]. Several different thermal property schemes are designed for this study based on the general variation range of these parameters, as shown in Table 6. For example, the general range of thermal conductivity is about 1.00–4.00 [34].

Table 6. Scheme design of different thermal parameters.

Parameters	Value			Unit
Thermal conductivity	1.00	2.51	4.00	W/(m·°C)
Rock grain specific heat	400	920	1200	J/(kg·°C)
Rock grain density	1000	2600	4000	kg/m^3

Fig. 14 shows the energy flow rate of different thermal conductivity, rock grain specific heat and rock grain density. Only a slight difference can be seen in Fig. 14between the energy flow rates under different parameters. The results indicate that the effective ATES can be achieved under normal formation properties.

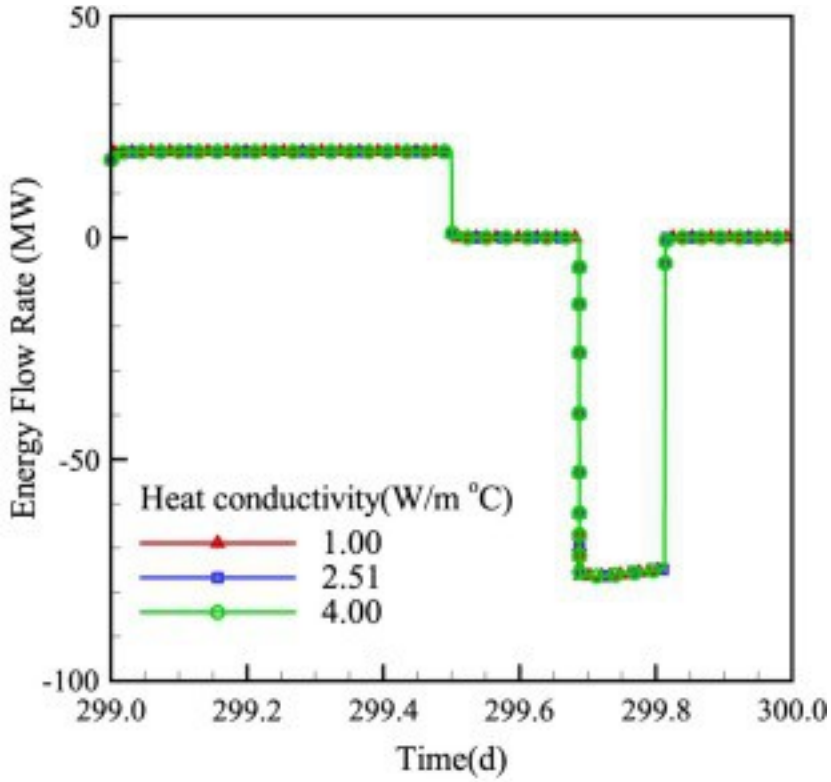
50
0
-50
-100
Energy Flow Rate (MW)
Heat conductivity(W/m °C)
1.00
2.51
4.00
299.0
299.2
299.4
299.6
299.8
300.0
Time(d)

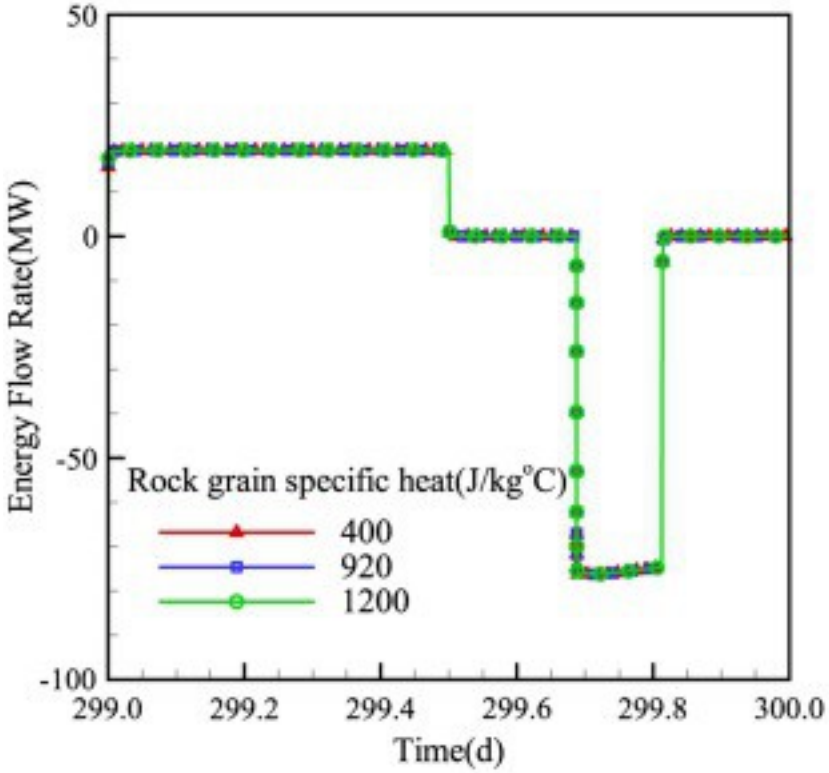
50
0
-50
-100
Energy Flow Rate(MW)
Rock grain specific heat(J/kg°C)
400
920
1200
299.0
299.2
299.4
299.6
299.8
300.0
Time(d)


50

1. Download high-res image (324KB)
2. Download full-size image

Fig. 14. Energy flow rate of different thermal conductivity, rock grain specific heat and rock grain density.

4.3. Impact of geothermal gradient and model uncertainly

The geothermal gradient varies from the locations. To investigate the impact of gradient, different schemes are designed as shown in Table 7. We use the same well-head temperature and different well-bottom temperature to represent the different geothermal gradient. The results are shown in Fig. 15.

Table 7. Schemes design of different geothermal gradient.

Parameters	Value				Unit
Well-head temperature	15	15	15	15	°C
Well-bottom temperature	30	40	50	70	°C
Geothermal gradient	18.75	31.25	43.75	68.75	°C/km

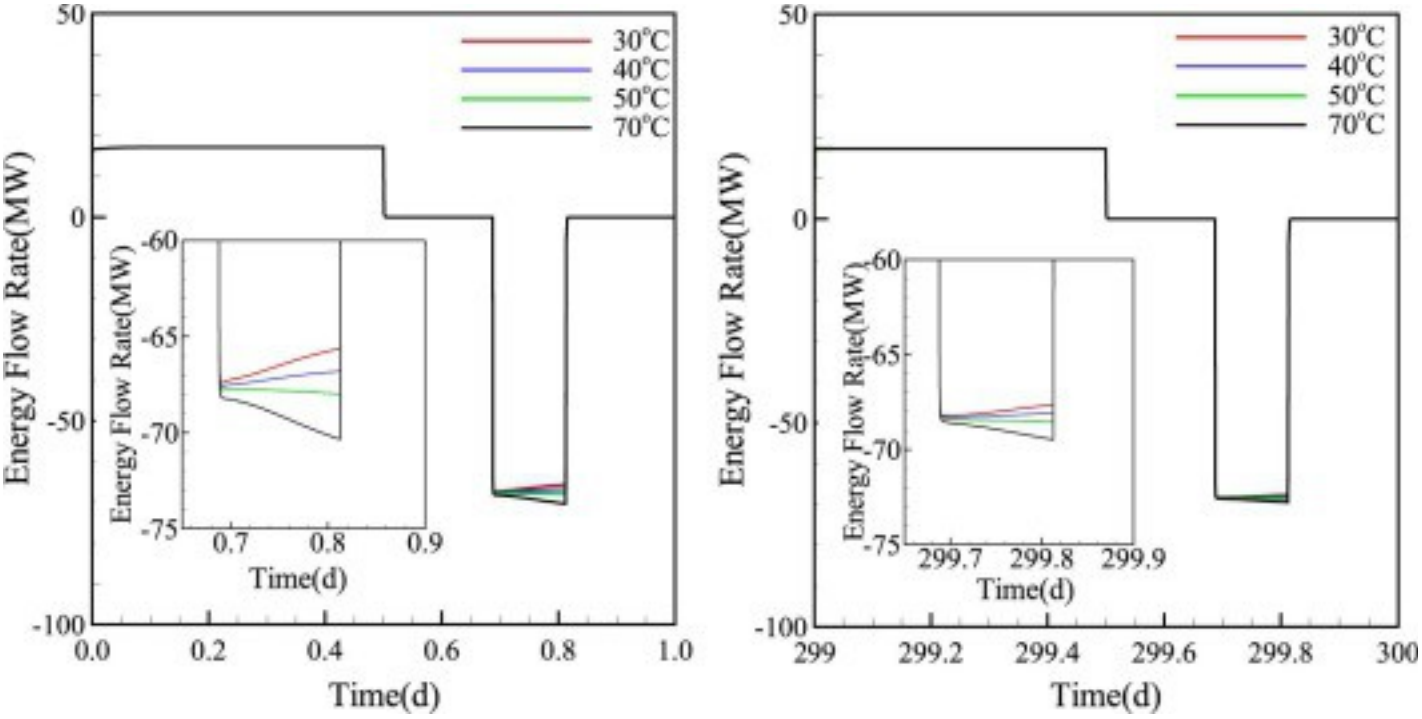

1. Download high-res image (125KB)
2. Download full-size image

Fig. 15. Energy flow rate of the first day (left) and the 300th day (right) for different geothermal gradient schemes.

The results confirmed the advantage of geothermal utilization is not obvious. In general, the energy flow rate under larger geothermal gradient is larger than under the lower

gradient. This advantage ease up as cycles continue as shown in the insert figure of Fig. 15. Overall, the amount of energy recovered mainly come from the energy injected. The energy loss to or get from the inherent geothermal energy only occupy a small part of total energy due to the slow heat transfer rate between compressed air and liquid water of the aquifer.
The proposed approach is expected to significantly improve the energy storage efficiency with only minor thermal storage cost. Use aquifer for thermal storage does not require either the high cost pressurized storage container and material, or drilling new boreholes. The boreholes for air injection and production in CAESA system are also used for heat storage operation. It is almost no additional cost to an original CAESA system, which is expected significantly lower the cost for TES with man-made containers, especially for large-scale heat storage.

The uncertainty of the simulation results comes from several aspects, such as the aquifers heterogeneity and ideal gas calculation error. Almost the aquifers in fields have heterogeneity and it will affect the pressure and temperature distribution as well as variation. Since our investigations focus on the foundation questions of CAESA and the real geological data differs from each other, we use the homogeneity model to investigate the system performance under ideal condition to in this study. Another uncertainty of our simulation results is the calculation error of compressed air as ideal gas. Despite the previous studies show not significant air properties error between ideal gas and real gas under low pressure and temperature, the uncertainty indeed would affect the final quantify data.

5. Conclusion

One integrated wellbore-reservoir numerical model was developed to investigate the impact of ATES on the performance of CAESA. Overall, the combination of CAESA and ATES can help to improve the performance of the CAESA system based on the simulation results. The aquifers act out as an ideal candidate for the thermal energy storage, which keeps higher energy recovery efficiency. In addition, the considerable utilization of geothermal energy by injecting cold air and producing hot air occurs only at the beginning of operations. The storage reservoir boundary permeability has a significant influence on the CAESA system performance. However, other reservoir properties, such as the storage reservoir permeability, thermal conductivity, rock grain specific heat and rock grain density) have little impact on storage capability.

In general for real CAESA project designing, several suggestions from this study can be used. First of all, injection temperature can be higher than the standard of CAESC. The energy recovery efficiency keeps still high among the usual aquifers. Another issue we should consider is the storage reservoir boundary permeability, which can significant affect the CAESA system performance. The optative formation for the CAESA system is with large storage reservoir permeability and low boundary permeability, which is analogous to a cavern but saturated with solid particles that hold heat.

However, there remain many challenges that should be considered during the design of CAESA systems. One important aspect that we care is the aquifer performance under high temperature (200–300 °C). Another inevitable aspect is the impact of high temperature on the processes of chemical reaction since many minerals consist the water and solid in aquifers. The reaction of O_2 in the compressed air with minerals should be further studied.

Acknowledgement

This research was granted funding by the Fundamental Research Funds for the Central Universities through Beijing Normal University (No. 2015KJJCB17). It was also supported by the China Scholarship Council (CSC) for the first author's visit to Lawrence Berkeley National Laboratory.

References

[1]

Yang B, Makarov Y, Desteese J, Viswanathan V, Nyeng P, McManus B, et al. On the use of energy storage technologies for regulation services in electric power systems with significant penetration of wind energy. In: 5th International conference on european electricity market, 2008 EEM 2008. IEEE; 2008. p. 1–6.

[2]

Crotogino F, Mohmeyer K-U, Scharf R. Huntorf CAES: more than 20 years of successful operation. AKE.

[3]

M. Raju, S.K. Khaitan**Modeling and simulation of compressed air storage in caverns: a case study of the Huntorf plant**

Appl Energy, 89 (2012), pp. 474-481

ArticleDownload PDFView Record in Scopus

[4]

Succar S, Williams RH. Compressed air energy storage: theory, resources, and applications for wind power. Princeton environmental institute report 2008;8.

[5]
J. Rutqvist, H.-M. Kim, D.-W. Ryu, J.-H. Synn, W.-K. Song**Modeling of coupled thermodynamic and geomechanical performance of underground compressed air energy storage in lined rock caverns**
Int J Rock Mech Min Sci, 52 (2012), pp. 71-81
ArticleDownload PDFView Record in Scopus
[6]
Xiaoying Z, Runqiu H, Chao L, Rabczuk T. A coupled thermo-hydro-mechanical model of jointed hard rock for compressed air energy storage. Math Probl Eng 2014:179169 (179111 pp.)–179169 (179111 pp.).
[7]
B. Kantharaj, S. Garvey, A. Pimm**Compressed air energy storage with liquid air capacity extension**
Appl Energy, 157 (2015), pp. 152-164
ArticleDownload PDFView Record in Scopus
[8]
R.D. Allen, T.J. Doherty, L.D. Kannberg**Summary of selected compressed air energy storage studies**
Pacific Northwest Labs, Richland, WA (USA) (1985)
[9]
R. Kushnir, A. Ullmann, A. Dayan**Compressed air flow within aquifer reservoirs of CAES plants**
Transp Porous Media, 81 (2010), pp. 219-240
CrossRefView Record in Scopus
[10]
C.M. Oldenburg, L. Pan**Porous media compressed-air energy storage (PM-CAES): theory and simulation of the coupled wellbore-reservoir system**
Transp Porous Media, 97 (2013), pp. 201-221
CrossRefView Record in Scopus
[11]
C.M. Oldenburg, L. Pan**Utilization of CO_2 as cushion gas for porous media compressed air energy storage**
Greenho Gases: Sci Technol, 3 (2013), pp. 124-135
CrossRefView Record in Scopus
[12]
Guo C, Zhang K, Li C. Influence of permeability on the initial gas bubble evolution in compressed air energy storage in aquifers. In: TOUGH symposium 2015. Berkeley, California; 2015.
[13]

C. Guo, K. Zhang, C. Li, X. Wang**Modelling studies for influence factors of gas bubble in compressed air energy storage in aquifers**
Energy, 107 (2016), pp. 48-59
ArticleDownload PDFView Record in Scopus

[14]

Jarvis A-S. Feasibility study of porous media compressed air energy storage in South Carolina, United States of America; 2015.

[15]

B. McGrail, J. Cabe, C. Davidson, F. Knudsen, D. Bacon, M. Bearden, *et al.***Technoeconomic performance evaluation of compressed air energy storage in the Pacific Northwest**
Pacific Northwest National Laboratory, Richland (2013)

[16]

M. Cai, K. Kawashima, T. Kagawa**Power assessment of flowing compressed air**
J Fluids Eng, 128 (2006), pp. 402-405
CrossRefView Record in Scopus

[17]

F. Buffa, S. Kemble, G. Manfrida, A. Milazzo**Exergy and exergoeconomic model of a ground-based CAES plant for peak-load energy production**
Energies, 6 (2013), p. 1050
CrossRefView Record in Scopus

[18]

N. Hartmann, O. Vöhringer, C. Kruck, L. Eltrop**Simulation and analysis of different adiabatic compressed air energy storage plant configurations**
Appl Energy, 93 (2012), pp. 541-548
ArticleDownload PDFView Record in Scopus

[19]

Crotogino F. Compressed air storage. Internationale Konferenz Energieautonomie durch Speicherung Erneuerbarer Energien; 2006.

[20]

M. Budt, D. Wolf, R. Span, J. Yan**A review on compressed air energy storage: Basic principles, past milestones and recent developments**
Appl Energy, 170 (2016), pp. 250-268
ArticleDownload PDFView Record in Scopus

[21]

L. Miró, J. Gasia, L.F. Cabeza**Thermal energy storage (TES) for industrial waste heat (IWH) recovery: a review**

Appl Energy, 179 (2016), pp. 284-301
ArticleDownload PDFView Record in Scopus

[22]

Z. Guo, G. Deng, Y. Fan, G. Chen**Performance optimization of adiabatic compressed air energy storage with ejector technology**
Appl Therm Eng, 94 (2016), pp. 193-197
ArticleDownload PDFView Record in Scopus

[23]

X. Luo, J. Wang, C. Krupke, Y. Wang, Y. Sheng, J. Li, *et al.***Modelling study, efficiency analysis and optimisation of large-scale adiabatic compressed air energy storage systems with low-temperature thermal storage**
Appl Energy, 162 (2016), pp. 589-600
ArticleDownload PDFView Record in Scopus

[24]

Zunft S, Jakiel C, Koller M, Bullough C. Adiabatic compressed air energy storage for the grid integration of wind power. In: Sixth international workshop on large-scale integration of wind power and transmission networks for offshore windfarms, Delft, The Netherlands; 2006.

[25]

S. Wang, X. Zhang, L. Yang, Y. Zhou, J. Wang**Experimental study of compressed air energy storage system with thermal energy storage**
Energy, 103 (2016), pp. 182-191
ArticleDownload PDFCrossRefView Record in Scopus

[26]

S.A. Zavattoni, M.C. Barbato, A. Pedretti, G. Zanganeh, A. Steinfeld**High temperature rock-bed TES system suitable for industrial-scale CSP plant – CFD analysis under charge/discharge cyclic conditions**
Energy Proc, 46 (2014), pp. 124-133
ArticleDownload PDFView Record in Scopus

[27]

G. Schout, B. Drijver, R. Schotting**The influence of the injection temperature on the recovery efficiency of high temperature aquifer thermal energy storage: comment on Jeon et al., 2015**
Energy, 103 (2016), pp. 107-109
ArticleDownload PDFView Record in Scopus

[28]

Crotogino F, Quast P. Compressed-air storage caverns at Huntorf. In: ISRM international symposium-rockstore 80. International Society for Rock Mechanics; 1980.

[29]

L. Pan, C.M. Oldenburg**T2Well—an integrated wellbore–reservoir simulator**

Comput Geosci, 65 (2014), pp. 46-55
ArticleDownload PDFView Record in Scopus

[30]

Pruess K, Oldenburg C, Moridis G. TOUGH2 user's guide version 2. Lawrence Berkeley National Laboratory; 1999.

[31]

C. Guo, L. Pan, K. Zhang, C.M. Oldenburg, C. Li, Y. Li**Comparison of compressed air energy storage process in aquifers and caverns based on the Huntorf CAES plant**
Appl Energy, 181 (2016), pp. 342-356
ArticleDownload PDFView Record in Scopus

[32]

Pan L. Wingridder-an interactive grid generator for TOUGH2. Lawrence Berkeley National Laboratory; 2003.

[33]

Bridger DW, Allen DM. Designing aquifer thermal energy storage systems; 2005.

[34]

Koňáková D, Vejmelková E, Černý R. Thermal properties of selected sandstones. In: Frederic Kuznik MR, Abdel-Badeeh M. Salem, editors. Proceedings of the 4th international conference on fluid mechanics and heat & mass transfer, Dubrovnik, Croatia. Advances in Mechanical Engineering; 2013.